F6

Pyroelectric Depth Profiles

**Heat Transport Phenomena
and Depth-Profiling of Pyroelectric Polymer Films Studied with the
Laser-Intensity Modulation Method (LIMM)**

Tutor: Dr. Axel Mellinger*

April 23, 2005

Contents

*Tel.: (0331) 977-1033, Email: axm@rz.uni-potsdam.de, Room 1.19.214

1 Introduction

In preparation for the experiment, careful reading of this manual is highly recommended. However, for the really impatient students, the most important paragraphs are highlighted by vertical black bars in the margin.

In the text, there are a few **Checkpoints** and **Problems**. Checkpoints test your understanding of the basic concepts; you should be prepared to answer the questions in the discussion with the instructor prior to the experiment. Problems treat certain aspects at greater depth; **their solutions should be included in the lab report**.

Use common sense in your data analysis! Always ask yourself if the results you obtain are physically meaningful.

Physical and Mathematical Concepts

- heat conduction
- bolometers
- pyroelectricity
- data acquisition / computer interfaces
- convolution/deconvolution (optional)

Equipment

- lock-in amplifier
- diode laser
- polymer films on sample holders
- Peltier cooler

Abstract

The macroscopic centro-symmetry of polymer films can be broken by subjecting the sample to a strong static electric field, generated e. g. by surface electrodes or from a corona discharge. These so-called *poled* polymers often show a large piezo- and/or pyroelectric effect, making them the material of choice in a large variety of applications, such as microphones, pressure sensors or infrared motion sensors [1]. To ensure uniform poling across the thickness of the polymer film (typically 5...100 µm), experimental methods for obtaining a depth-profile of the piezo- or pyroelectric coefficient are necessary [2]. For pyroelectric polymer films, where a temperature variation induces a change in surface charge, the **L**aser-**I**ntensity **M**odulation **M**ethod (LIMM) is an easily implemented way of measuring pyroelectric distributions with a resolution of approximately 1 µm. With a focused laser beam, the same technique can be used to implement a scanning pyroelectrical microscope [3].

An intensity-modulated diode laser illuminates an opaque front electrode on the polymer film, creating a temporal and spatial thermal wave inside the sample (Fig. 1). At low modulation frequencies (10 Hz or less), the sample is heated and cooled homogeneously, so that layers at all depths contribute to the pyroelectric current (provided they have a non-zero pyroelectric coefficient). At high frequencies (100 kHz) the penetration depth becomes less than 1 µm, and we are looking at the pyroelectric behavior of a thin layer only.

Absolute calibration of the pyroelectric depth-profiles requires knowledge of the laser-induced temperature change at the front and rear surface of the sample. Small temperature

Electrodes

Laser
Diode

Intensity−modulated Light

Polymer

Function
Generator

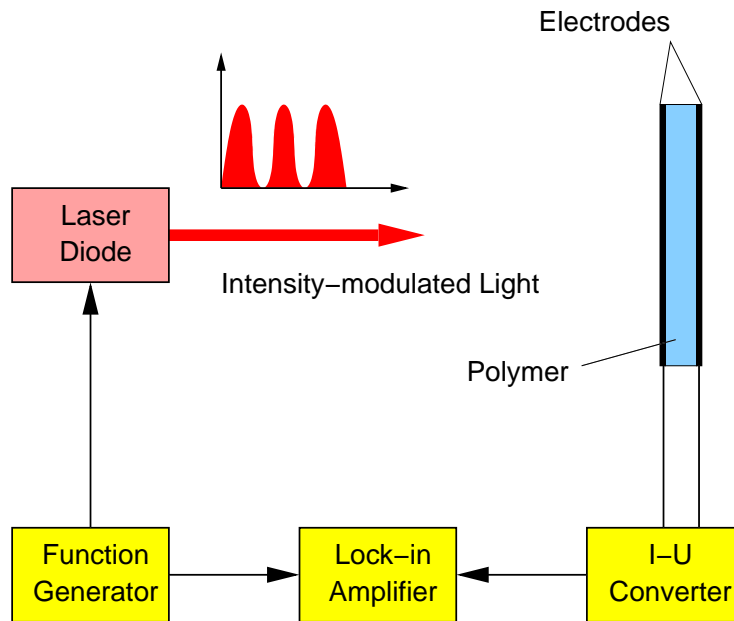Lock−in
Amplifier

I−U
Converter

Figure 1: Schematic setup of a LIMM experiment (adapted from [4]).

changes can be detected with a bolometric technique, where the resistance of the aluminum surface electrode is measured.

The experiment includes the following steps:

1. Bolometer calibration by measuring the voltage across the surface electrode at different temperatures.

2. Measurement of the transient (laser-induced) temperature at both surfaces and calculation of the thermal diffusivity.

3. Measurement of the frequency-dependent pyroelectric current of several samples. Calculation of the depth-profile of the pyroelectric coefficient. A few specially prepared samples (bimorph, single pyroelectric layer) have to be identified. With the surface temperature obtained in step 2 it is possible to calculate the absolute value of the pyroelectric coefficient.

Related Techniques, Further Reference

The thermal wave method is only one of several techniques developed for investigating pyroelectric depth-profiles. For example, pulsed lasers have been used instead of modulated cw lasers to generate a time-dependent temperature step or pulse in the sample. Refer to [2] for further references to pyroelectric measurement techniques.

An illustrated introduction into the LIMM technique is given at

        http://canopus.physik.uni-potsdam.de/research/limm/limm_main.html

2 Experiment

2.1 Samples

The pyroelectric polymer films used in the present experiment are made of polyvinylidene fluoride (PVDF). With its $-[CH_2-CF_2]-$ repeat unit, it is chemically related to polyethylene ($-[CH_2]-$) and polytetrafluoroethylene ($-[CF_2]-$). Due to the electronegativity of the fluorine atoms, the CF_2 groups carry a dipole moment. However, this does not necessarily translate into a macroscopic polarization, unless the molecular dipole units are all oriented in the same direction. PVDF is a semicrystalline polymer with at least four crystalline modifications. The two most important ones are the α and the β phase. In the α phase, the molecular chains form loose spirals so that the dipole moments in a unit cell cancel. In the zigzag-shaped β phase (Fig. 2), all dipoles in a crystallite are aligned in parallel, resulting in a nonzero polarization. From the melt, PVDF crystallizes into the nonpolar α phase, which is the most stable phase at room temperature. Mechanical stretching, high-field poling or annealing at high temperature is necessary to obtain the polar β phase.
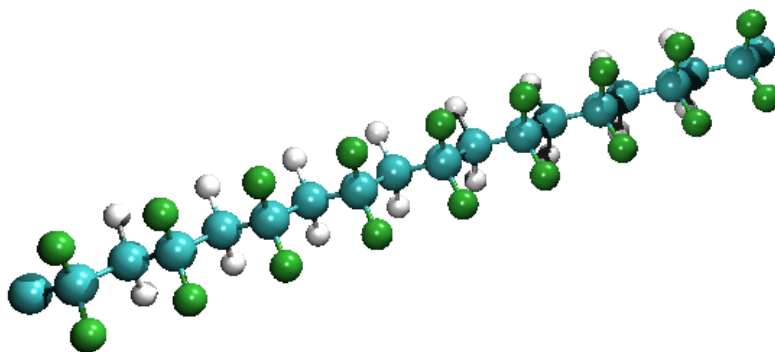

Figure 2: The β phase of PVDF.

Even in the polar β phase, different molecular chains are oriented randomly with respect to each other. Consequently, the polymer does not have a net polarization and does not exhibit piezo- or pyroelectric behavior. However, by applying an external electric field, the molecular dipoles can be oriented with the result of PVDF becoming both piezo- and pyroelectric (Fig. 3). This process is known as *poling*. The samples used in the experiment have been poled in a corona discharge running at approx. 12 kV.

2.2 Simulations

Before you start experimenting with real polymer samples, you should run a few numerical simulations to familiarize yourself with the data analysis techniques. We have provided a
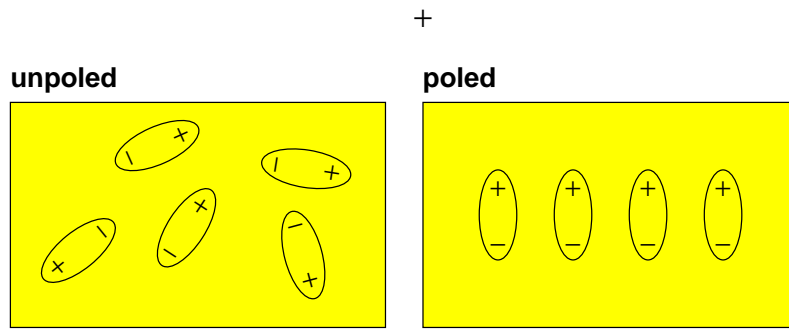
Figure 3: Orientation of molecular dipoles before and after poling.

set of programs for the ***Octave*** programming environment on a Linux Workstation. The screen-shot in Fig. 4 shows the desktop screen. There are three windows: one ***Octave*** shell, one graphics output, and an `xterm` window with the text editor `joe` running. You can switch between windows by clicking on the window to be activated with your mouse pointer. Please refer to the Appendix C for a brief description of ***Octave*** and the text editor.
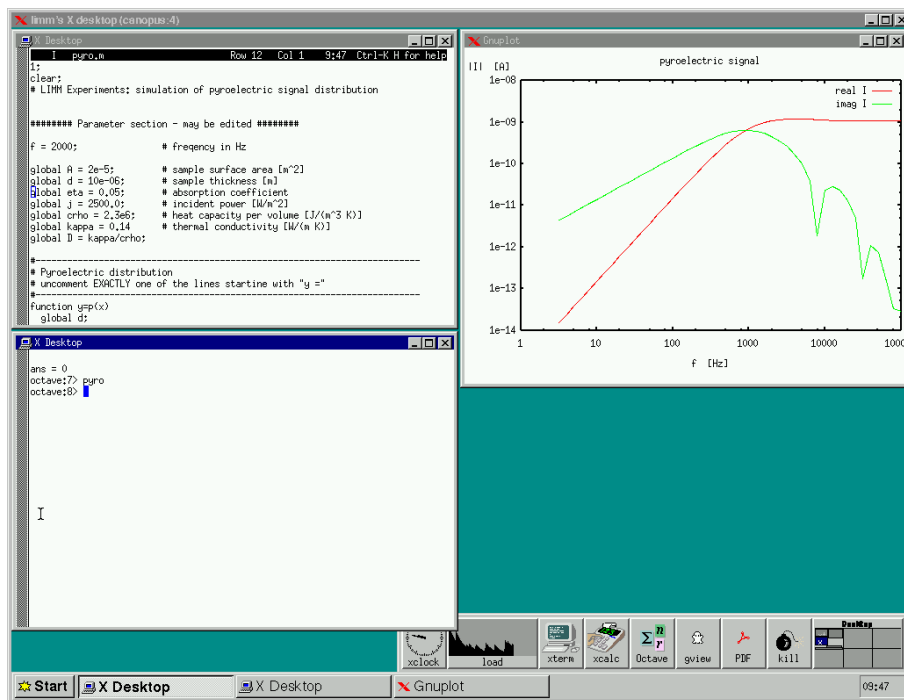

Figure 4: Screen-shot of the ***Octave*** environment.

You should run the following simulations:

- Determine the temperature distribution at different frequencies using the program

temperature. The lock-in amplifier will handle frequencies between 0.5 Hz and
100 kHz.

- Simulate the pyroelectric current as a function of frequency for different functional
  forms of the pyroelectric coefficient. Some functions have already been defined in
  the source code pyro.m and can be activated by removing the comment sign # at
  the beginning of the line. You are, of course, welcome to add your own functions.

- Once you have run pyro, run reconstruct to calculate the distribution of the py-
  roelectric coefficient from the pyroelectric current. Note the very different results of
  the approximation and the regularization technique.

2.3   Setup

The basic setup is shown in Figures 5 through 7. The polymer film has thin (50 nm)
aluminum electrodes on both sides which also serve as opaque light absorbers. Four
connector pads are needed for the bolometric experiments. The polymer film is mounted
on a carrier consisting of two epoxy plates. Care should be taken not to touch the thin
polymer film. The carrier can be mounted upside down, allowing LIMM experiments on
either surface of the polymer. The carrier plate fits on top of the water-cooled Peltier
cooling/heating block. A ribbon cable connects the sample carrier to the BNC sockets on
the left side of the cell. The whole unit is mounted on a x-y translation stage, which is
operated by four adjustment screws. These screws work in pairs, i. e. one screw must be
loosened while the opposite screw is tightened, and vice versa. The cell is flushed with
dry nitrogen gas to prevent condensation on the cold surfaces.
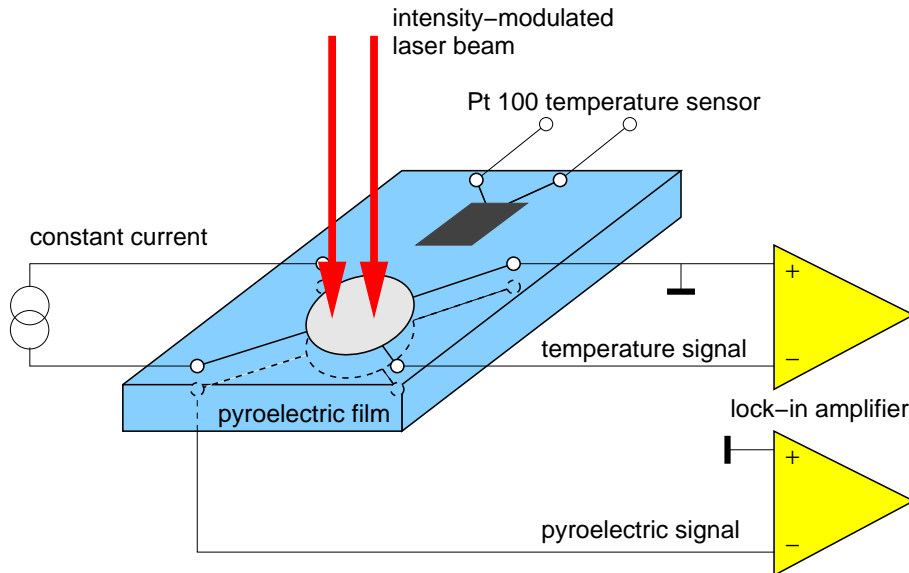
Figure 5: Setup for LIMM and bolometric measurements.

diode laser

detachable front plate

laser interlock

ITO window

BNC sockets

copper plate

Peltier stage

Figure 6: Front view of the sample cell.

diode laser

detachable
front plate

bolometer

| Peltier | | Pt 100 | I | V | Pyro |

+   −

cooling water

copper plate

Peltier stage

Figure 7: Side view of the sample cell.

2.4 Data Acquisition

To record the frequency dependence of the bolometer voltage and pyroelectric current you must set the laser modulation frequency and read out the lock-in amplifier. You have two options:

1. Select the frequencies using the push-buttons on the front panel, read out the real and imaginary part of the signal from the corresponding display, and enter them manually into the computer. This approach requires no programming skills, but is rather time-consuming. To be able to use the `analyze` routine (cf. Tab. 1), the data must b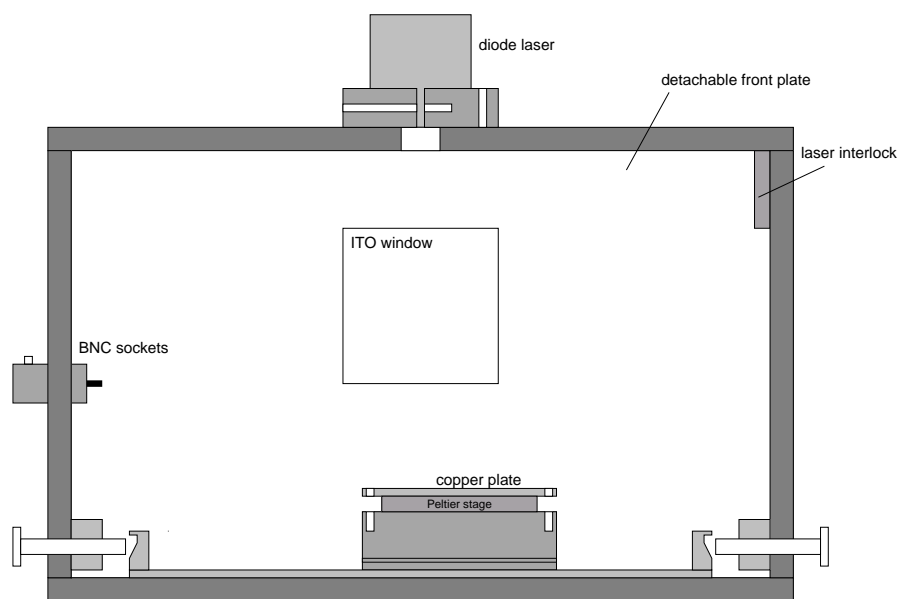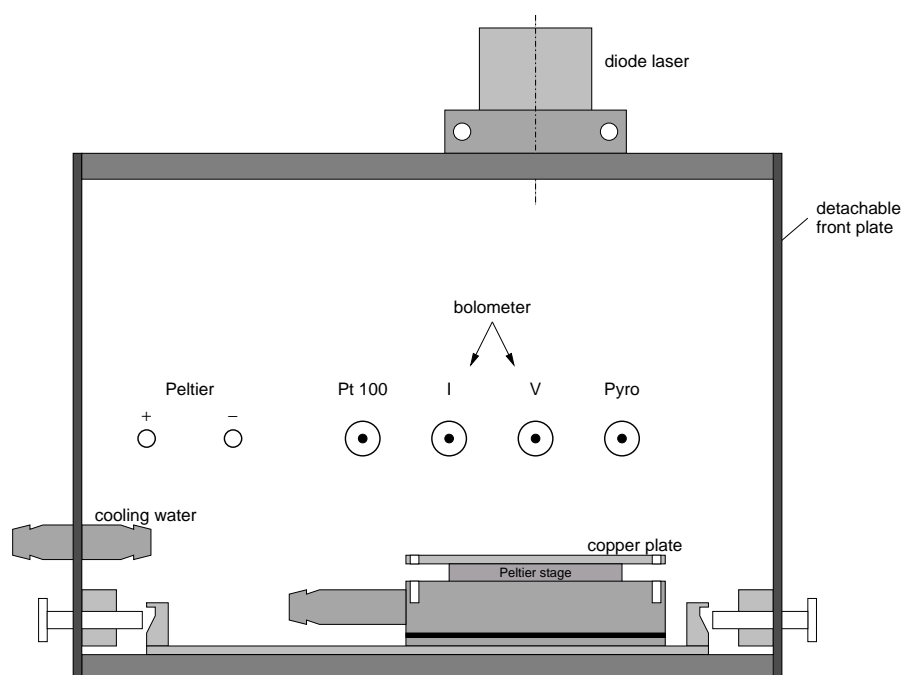e written in three columns containing the frequency (in Hz) and the real and imaginary part of the pyroelectric current, respectively. Use blanks or tabs to separate the columns.

2. Use the `limmdac` data-acquisition program that automatically scans the frequency and reads out data via the RS 232 serial interface. As a programming exercise, it is your task to complete a loop structure in the main program that sets the oscillator frequency of the lock-in amplifier. Interfacing laboratory equipment to a computer is a common task in setting up an experiment, so we recommend that you follow this approach. Please refer to Appendix C for programming instructions.

2.5 Running the Experiment

1. **Bolometer calibration.** In the first part of the experiment we shall investigate the propagation of the thermal wave through the sample. Thus, we need to measure the transient (time-dependent) temperature at the front and back surface. Moreover, we will learn in section 3.4 that the temperature amplitude at the front surface of the sample must be known in order to obtain absolute pyroelectric coefficients. Since ordinary thermometers are not fast enough to follow the laser-induced temperature oscillations, we will use the surface electrode as a *bolometer* that changes its conductivity as a function of temperature. The conductivity is measured by feeding a small current (10 mA) through two of the four connectors while measuring the voltage drop across the other two connectors with a voltmeter (Fig. 5).

   Checkpoint 1 *What is the advantage of the four-point method for measuring the conductivity of the aluminum electrode? Wouldn't an ohmmeter hooked up to two of the four connectors be sufficient? (Hint: consider the effects of parasitic resistance in the cables.) Why are we using a battery pack instead of a standard power supply as constant current source?*

   To make quantitative measurements, we first need to calibrate the bolometer, i. e. determine the relation between voltage drop across the electrode and temperature. This is done by heating the sample to a number of different temperatures and, with the laser turned off, measuring the DC voltage drop with a multimeter. An independent temperature measurement is simultaneously done with a Pt 100 sensor. The

Pt 100 has a nominal resistance of 100 Ω at 0 °C, which increases with temperature. Using a reference table, the measured resistance can be converted to temperature.

Insert sample holder #1 and connect the ribbon cable. Keep the laser turned off. Turn on the cooling water (a small flow rate is sufficient) and the nitrogen gas flow. Insert sample #1. Connect an Ohmmeter to the "Pt 100" BNC connector and a voltmeter to the "V" connector. Connect the battery pack (8 "D" cells) to the "I" BNC connector via the voltage stabilizer. **Note: To extend the life of the battery pack, please disconnect it from the stabilizer when you are done with the bolometer experiments.**

Cooling/heating: Connect the Peltier power supply (the large box to your left). Applying "+" polarity to the red connector will cool the sample. A minimum temperature of approx. −25 °C can be reached at a Peltier current of $I_{\mathrm{Pelt}} = +4$ A. Applying "−" polarity to the red connector will heat the sample. A maximum temperature of approx. +45 °C can be reached at $I_{\mathrm{Pelt}} = -1$ A.

Caution: Do not exceed the maximum current of 4 A in the cooling mode and 1 A in the heating mode! Damage to the Peltier cooler may occur otherwise. Check the cooling water before turning on the Peltier current.

With the bolometer current set to 10 mA, measure the voltage drop across the bolometer and the Pt 100 resistance in the temperature range between −20 °C and +40 °C. Note that the cables leading to the Pt 100 have a resistance of $R_0 = 0.30\ \Omega$, which must be subtracted from the measured value. Use the supplied reference table [5] (you will need to interpolate between tabulated values) or the online Pt 100 calculator (`http://www.isotech.co.uk/prtcalc-web.html`) to convert the measured Pt 100 resistance to temperature. Make a graph of the calibration curve (bolometer voltage vs. temperature). Use a least squares fit to determine the temperature coefficient

$$\alpha_{\mathrm{bol}} = \frac{\partial V}{\partial T} \tag{1}$$

which is needed in the following step.

When you are done with the calibration, measure the voltage drop at room temperature with the diode laser on and off, respectively. Find out how much the sample temperature is increased by the cw laser beam. **Turn off the nitrogen gas and cooling water.**

2. **Transient surface temperature:** As in the previous step, a constant current (from the battery pack) flows through the top electrode. This time, however, the central spot is heated by the modulated laser beam, causing a time-dependent voltage drop across the other two connectors which is measured with the lock-in amplifier. With the bolometer calibrated in the previous step, we can thus measure the transient temperature $\Delta T_\sim$ at the top electrode.

Turn on the laser. Adjust the translation stage so that the laser beam hits the center of the metallized electrode. Set the internal oscillator of the lock-in amplifier to approx. 3 Hz. Connect the "Channel A" lock-in amplifier input to the "V" BNC socket. You should see an imaginary (90° phase-shifted) signal of a few µV. Record

the frequency dependence of the bolometer voltage between 1 and 1000 Hz. Here, you may use the `limmdac` data acquisition program, described in Appendix C.1.1.

Close the shutter (using the knob on the top side of the chamber) and perform a *null measurement*. Ideally, the null measurement should produce no signal, but due to internal offsets in the lock-in amplifier a non-zero voltage is often seen at higher frequencies. For further analysis, this null measurement must be subtracted (separately for the real and imaginary part) from the open shutter measurement.

Using calibration coefficient α_{bol} from the previous step, plot the transient temperature $\Delta T_\sim$ at the top electrode versus frequency in a double-log diagram. Confirm that at low frequencies the real part of $\Delta T_\sim(x = 0)$ is much smaller than the imaginary part. For the imaginary part, compare the result with the $\omega^{-1/2}$ and ω^{-1} behavior predicted by Eqs. (9) and (10) for high and low frequencies, respectively.

Checkpoint 2 *Why does the curve deviate from Eq. (10) below 2 Hz?*

Turn sample #1 upside down **without unplugging the ribbon cable** and record the temperature at the rear electrode (including the null measurement). Calculate the phase lag between the temperature at the front and rear electrode (cf. Appendix E for details) and determine the thermal diffusivity D of the sample by fitting Eq. (13) to the phase lag data.[1] Compare your result with the diffusivity calculated from the material parameters in Appendix B.

3. **Pyroelectric signal:** Remove all connections to the sample cell. Turn the sample so that the side of the ribbon cable labeled "top" is really on top. Connect the input of current-to-voltage (I-U) converter (gain 20 MV/A) to the "Pyro" BNC socket on the left side of the sample cell and its output to the "Channel A" input of the lock-in amplifier. Turn on the laser. Measure the pyroelectric signal at frequencies between 10 Hz and 100 kHz at the top sample surface.

Turn the sample upside down, **leaving the ribbon cable connected**. Now measure the frequency dependence of pyroelectric signal "from the other side".

Use the approximation and regularization method to reconstruct the distribution of the pyroelectric coefficient. Plot the data from both sides into a single diagram, using $d - x$ instead of x as the abscissa of the rear surface data. The thickness of polymer film is written on the sample holder.

Use Eq. (33) to calculate the average pyroelectric coefficient of the sample. For this task, you need the surface temperature (from the previous step) and the pyroelectric current at a common frequency where Eq. (10) holds. Estimate the error of the result. Make a calibrated plot of the pyroelectric depth profile.

Insert samples #2 and #3, record their pyroelectric signal and calculate the depth-profile of the pyroelectric coefficient. (Since no surface temperature was recorded for these samples, you will only obtain their relative depth profiles.) One of the samples is a *bimorph* (a sandwich of two films with opposite polarization). Which one? What is the likely composition of the other samples?

---

[1]This requires data analysis software capable of a *non-linear least squares fit*, such as GNUPLOT or ORIGIN.

Once you have an idea about the shape of the pyroelectric profile you should go back to the simulation and check whether this profile reproduces the measured pyroelectric signal.

At the end of your experiments, make sure that the battery pack has been disconnected. Unplug the power supplies of the diode laser and the current-to-voltage converter.

3 Theoretical Background

This manual gives the basic theoretical framework of the LIMM experiment. For a more detailed description of the mathematical analysis, see Refs. [6, 7]. An online introduction to the LIMM method with animaged image sequences can be found at

> http://canopus.physik.uni-potsdam.de/research/limm/limm_main.html
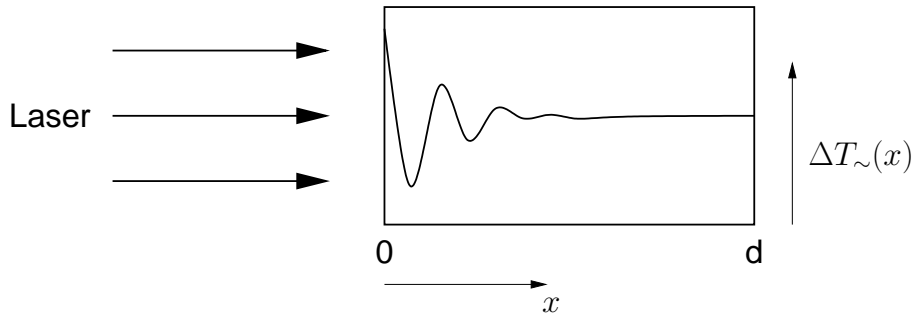
3.1 Heat Conduction

Figure 8: Thermal wave inside the sample.

Figure 8 shows a sample of thickness d, which is illuminated from the $x = 0$ side by a sinusoidally modulated laser beam with a time-dependent intensity

$$j = j_0 + j_\sim\, e^{i\omega t} = j_0 + j_\sim\, e^{2\pi i f t} \, , \tag{2}$$

where f is the modulation frequency.[2] A fraction η of the light is absorbed and heats up the sample. The temperature distribution inside the polymer film is given by the one-dimensional heat-conduction equation (also known as *Fick's law*):

$$\kappa \frac{\partial^2 \Delta T(x,t)}{\partial x^2} = c\rho \frac{\partial \Delta T(x,t)}{\partial t} \, . \tag{3}$$

Here, $\Delta T(x,t)$ is the transient temperature distribution, κ the thermal conductivity [$\mathrm{W\,m^{-1}\,K^{-1}}$], c the heat capacity per unit mass [$\mathrm{J\,kg^{-1}\,K^{-1}}$] and ρ the mass density. The last three material constants are often combined into the *thermal diffusivity* $D = \kappa/(c\rho)$ [$\mathrm{m^2\,s^{-1}}$]. Note that Eq. (3) only describes the *time-dependent* part of the solution. The complete solution contains a time-independent term which is a function of the average laser intensity j_0. Since we heat the front surface of the sample and have thermal losses (through thermal conductivity, radiation and convection) at the rear side and edges of the heated area, a temperature gradient will form inside the polymer. However, it is stationary and does not contribute to the pyroelectric current. On the other hand, the

---

[2]For reasons of simplicity, ω will sometimes be called "modulation frequency" even though the laser is modulated at $f = \omega/(2\pi)$.

time-dependent term in Eq. (2) produces *no net energy flow* into the sample. For sufficiently high modulation frequencies $\omega/(2\pi)$ (which, in practice, means more than a few Hz), thermal losses can be neglected.

Problem 1 *Derive the one-dimensional heat conduction equation! Hint: consider a slab of cross section A and calculate the energy gain and loss for a thin slice with a thickness dx.*

The solution of the heat conduction equation is subject to the following boundary conditions:

1. At the heated side,
$$\kappa \left. \frac{\partial \Delta T(x,t)}{\partial x} \right|_{x=0} = -\eta j_\sim e^{i\omega t} \ . \tag{4}$$

2. At the opposite side, there is no *time-dependent* heat flow (see the discussion in the previous paragraph). Consequently, the temperature gradient has to vanish, i. e.
$$\kappa \left. \frac{\partial \Delta T(x,t)}{\partial x} \right|_{x=d} = 0 \tag{5}$$

Experimentally, the second boundary condition can be fulfilled by using a free-standing sample (i. e., one that is not attached to a substrate). With these boundary conditions, Eq. (3) is solved by

$$\Delta T(x,t) = \Delta T_\sim(x)e^{i\omega t} = \frac{\eta j_\sim}{\kappa k} \frac{\cosh[k(d-x)]}{\sinh(kd)} e^{i\omega t} \ . \tag{6}$$

$$k = (1+i)k_r \tag{7}$$

$$k_r = \sqrt{\omega/2D} \tag{8}$$

The penetration depth x_r of the thermal wave into the sample is given by the inverse of the thermal wave vector k_r. $\Delta T_\sim(x)$ is a complex quantity, indicating that the temperature oscillation inside the sample may be phase-shifted with respect to the laser beam.

Checkpoint 3 *What is the spatial resolution of LIMM if the modulation frequency can be tuned from 10 Hz to 100 kHz? (Hint: Use the material constants of polyvinylidene fluoride (PVDF) in Appendix B to calculate the penetration depth for a frequency of 10 Hz and 100 kHz.)*

Problem 2 *Show that Eq. (6) is approximated by*

$$\Delta T_\sim(x) = \frac{\eta j_\sim}{\kappa k} e^{-kx} \ . \tag{9}$$

for high frequencies ($k_r \gg d^{-1}$). This approximation will later be needed for the analysis of experimental LIMM data. For a PVDF sample with $d = 20$ µm, what is the minimum frequency above which Eq. (9) is valid ($k_r^{-1} < d/3$)?

Eq. (9) shows that the imaginary part of k determines the spatial oscillation of the thermal wave (similar to the wave vector of an electromagnetic wave), while the real part describes the damping of the thermal wave with increasing depth.

Problem 3 *Use Eqs. (6) and (9) to explain the nearly constant temperature in a wine cellar. Assume a thermal conductivity of $\kappa = 1.0$ W m^{-1} K^{-1}, an average depth of 3 m, a diurnal temperature amplitude of 5 K and an annual amplitude of 15 K. The heat capacity of the soil is approximately 0.9 J g^{-1} K^{-1}; its density 2.0 g cm^{-3}. Consider the soil only; neglect the presence of air in the wine cellar.*

At low frequencies ($k_r \ll d^{-1}$), the first-order approximation

$$\Delta T_{\sim}(x) = -i\,\frac{\eta j_{\sim}}{c\rho d}\,\frac{1}{\omega} \tag{10}$$

holds (note that the solution is constant across the sample thickness). In section 3.4 we will need this approximation for the calibration of the pyroelectric spectra. However, thermal losses limit the validity of Eq.(10) to frequencies above approx. 1 Hz.

Calculating the thermal diffusivity

The thermal diffusivity can be obtained from the transient temperature of the front and rear surface in the following way: The phase lag between the two transient temperatures is given by

$$\Delta\phi(\omega) \;=\; \arg\left(\frac{\Delta T_{\sim}(x = 0)}{\Delta T_{\sim}(x = d)}\right) \tag{11}$$

$$\;=\; \arg[\cosh(kd)]\,. \tag{12}$$

To avoid dealing with complex numbers, Eq. (12) can be rewritten as

$$\tan(\Delta\phi(\omega)) \;=\; \tanh(k_r d)\tan(k_r d)$$

$$\;=\; \tanh\left(\frac{d}{\sqrt{2D}}\sqrt{\omega}\right)\tan\left(\frac{d}{\sqrt{2D}}\sqrt{\omega}\right)\,. \tag{13}$$

At high frequencies, $\tanh(k_r d) \to 1$ and Eq. (13) can be approximated by

$$\Delta\phi \approx \frac{d}{\sqrt{2D}}\sqrt{\omega}\,. \tag{14}$$

For details on how to calculate $\Delta\phi$ from experimental temperature data, plese consult Appendix E.

3.2   Pyroelectric Current

Now that we know the temperature distribution inside the sample, we can calculate the pyroelectric signal generated by the oscillating temperatures. The experimental pyroelectric coefficient

$$p = \frac{1}{A}\frac{\partial Q}{\partial T} \tag{15}$$

describes the change ΔQ in surface charge resulting from a temperature change ΔT. The exact description of all first-order terms contributing to the pyroelectric coefficient is given by

$$r(x) = \alpha_p P(x) - (\alpha_x - \alpha_\epsilon)\epsilon_0 \epsilon E(x) , \tag{16}$$

where ϵ_0 is the permittivity of vacuum, ϵ the relative permittivity of the sample and $E(x)$ the electric field. The three coefficients α_p, α_x and α_ϵ denote the relative temperature dependencies of the polarization, the thermal expansion and the permittivity, respectively. If the polarization is locally compensated by a charge density $\rho(x)$, Eq. (16) reduces to [6]

$$r(x) = \alpha_p P(x) \equiv p(x) \tag{17}$$

The contribution to the pyrocurrent from a thin slice dx of the sample depends on the local pyroelectric coefficient $p(x)$ and the rate of change of the transient temperature. If we want to calculate the pyrocurrent measured between the electrodes on the end surfaces, we have to integrate over the sample thickness d:

$$I(t) = I_\sim\, e^{i\omega t} = \frac{A}{d}\ \int_0^d p(x)\frac{\partial \Delta T(x,t)}{\partial t}\ dx . \tag{18}$$

Inserting the temperature profile from Eq. (6) into Eq. (18), we obtain

$$I_\sim = \frac{A}{d}\frac{\eta j_\sim}{c\rho}\frac{k}{\sinh(kd)}\int_0^d p(x)\cosh[k(d-x)]\,dx . \tag{19}$$

In a LIMM experiment, one measures the pyroelectric current $I_\sim$ as a function of the modulation frequency ω. How then can we retrieve the pyroelectric coefficient $p(x)$ buried in the integral on the right hand side of Eq. (19)? It turns out that this is a non-trivial problem. To mathematicians, Eq. (19) is a Fredholm integral equation of the first kind. In the world of physics, these integral equations are *convolution integrals*

$$g(y) = \int f(x)r(y-x)dx , \tag{20}$$

where an "ideal" function $f(x)$ is convolved (which, in practice, means "smeared") with a response function $r(x)$.

One highly publicized example of such a response function was the flawed mirror of the Hubble Space Telescope (HST). After its launch in 1990 astronomers quickly realized that due to an incorrectly figured primary mirror, the nearly pinpoint star images (with a resolution of about 0.01 arcseconds) were "smeared out" to fuzzy blobs 0.6 arcseconds in diameter[3]. The problem the Hubble scientists were facing was similar to ours: how

---

[3]This problem was fixed during the first service mission in December 1993

to retrieve the "ideal" image $f(x)$ when only the blurred image $g(x)$ and the response function $r(x)$ are known.

Mathematically, this problem is easily solved. The convolution theorem states that

$$G(y) = F(y)R(y) \; , \tag{21}$$

where F, G and R are the Fourier transforms of the functions in Eq. (20). It seems that all we have to do is to calculate the Fourier transforms of $g(x)$ and $r(x)$, divide $G(y)$ by $R(y)$ and apply an inverse Fourier transformation to the result. In practice, however, this is a very ill-conditioned problem. Given the fact that $g(x)$ always contains some experimental noise, there is an infinite set of functions $f(x)$ which, after convolution with $r(x)$, agree with $g(x)$ within the experimental uncertainty. Going back to our original problem of solving Eq. (19), simple application of Fourier transforms would most likely yield a strongly oscillating result $p(x)$ which has nothing to do with the true distribution of the pyroelectric coefficient.

To obtain a meaningful solution of Eq. (19), there are several strategies, each with its own advantages and disadvantages. Two will be discussed in detail:

1. **Regularization techniques.** The above-mentioned ambiguities can be removed by introducing additional constraints. For example, if we seek to obtain a smooth function, we would require that the integral over the second derivative be as small as possible, i. e.

$$\int_0^d |p''(x)|^2 \, dx \stackrel{!}{=} \mathrm{Min.} \tag{22}$$

This technique is described in detail in Ref. [7]. A disadvantage is that one has to find the right compromise between suppressing unphysical oscillations and smoothing out the solution too much. In practice, one often encounters a strongly polarized layer near the surface (giving rise to a rapidly changing $p(x)$) and a much smoother distribution deep inside the sample, which is not handled very well by this particular type of regularization. A brief introduction into linear regularization techniques is given in Appendix F.

Another approach is to maximize the *entropy* instead of minimizing the second derivative. These *maximum entropy* techniques are widely used in image restoration.

2. **Approximation technique.** The above described techniques often produce artifacts or require a large computational effort. Near the surface of the sample, an approximate solution of the heat conduction equation can be used to obtain an analytical expression for the pyroelectric coefficient [6]. This method is discussed in detail in the following section.

3.3   Approximate Calculation of the Depth Profile of the Pyroelectric Coefficient

Now we come back to the approximate solution (9) of the heat conduction equation. Inserting this approximation into Eq. (18), we obtain

$$I_\sim = \frac{\eta j_\sim A}{c\rho d} \int_0^\infty p(x) k e^{-kx}\, dx \ . \tag{23}$$

Since $p(x) = 0$ outside the sample, the upper integration limit was changed to ∞ without affecting the result. Splitting this result into its real and imaginary parts yields

$$\Re I_\sim = \frac{\eta j_\sim A}{c\rho d} \int_0^\infty p(x) k_r [\cos(k_r x) + \sin(k_r x)] e^{-k_r x}\, dx \ , \tag{24}$$

$$\Im I_\sim = \frac{\eta j_\sim A}{c\rho d} \int_0^\infty p(x) k_r [\cos(k_r x) - \sin(k_r x)] e^{-k_r x}\, dx \ . \tag{25}$$

We now define the *penetration depth*

$$x_r = 1/k_r = \sqrt{2D/\omega} \tag{26}$$

and the function

$$p_a(x_r) = \frac{c\rho d}{\eta j_\sim A} \left[(\Re - \Im) I_\sim(\omega = 2D/x_r^2) \right] \ . \tag{27}$$

Inserting Eq. (24) and (25) we obtain

$$p_a(x_r) = \int_0^\infty p(x) \frac{2}{x_r} \sin\left(\frac{x}{x_r}\right) e^{-x/x_r}\, dx \ . \tag{28}$$

This is an integral equation with the kernel

$$f_a(x, x_r) = \frac{2}{x_r} \sin\left(\frac{x}{x_r}\right) e^{-x/x_r} \ , \tag{29}$$

which vanishes for both $x = 0$ and $x \to \infty$ and has the property

$$\int_0^\infty x^n f_a(x, x_r)\, dx = x_r^n \qquad \text{for } n \in \{0, 1, 2\} \ . \tag{30}$$

Therefore, $f_a(x, x_r)$ is a normalized scanning function which retrieves an approximate value of $p(x)$ at the location $x = x_r$. In particular, it *exactly* retrieves the coefficients of a Taylor expansion up to the second order. We can thus regard $p_a(x_r)$ as an approximation to the true distribution $p(x)$.[4] The penetration depth x_r is directly related to the modulation frequency ω through Eq. (26).

The spatial resolution at a given depth x_r is determined by the width of the kernel $f_a(x, x_r)$. Figure 9 shows that the resolution increases as we move closer to the heated surface of the sample (which is equivalent to increasing the frequency ω). Beyond the center of

---

[4]If Eq. (30) was true for all $n \geq 0$, we would have $p_a(x) = p(x)$, and the kernel $f_a(x, x_r)$ would be the delta function $\delta(x - x_r)$.
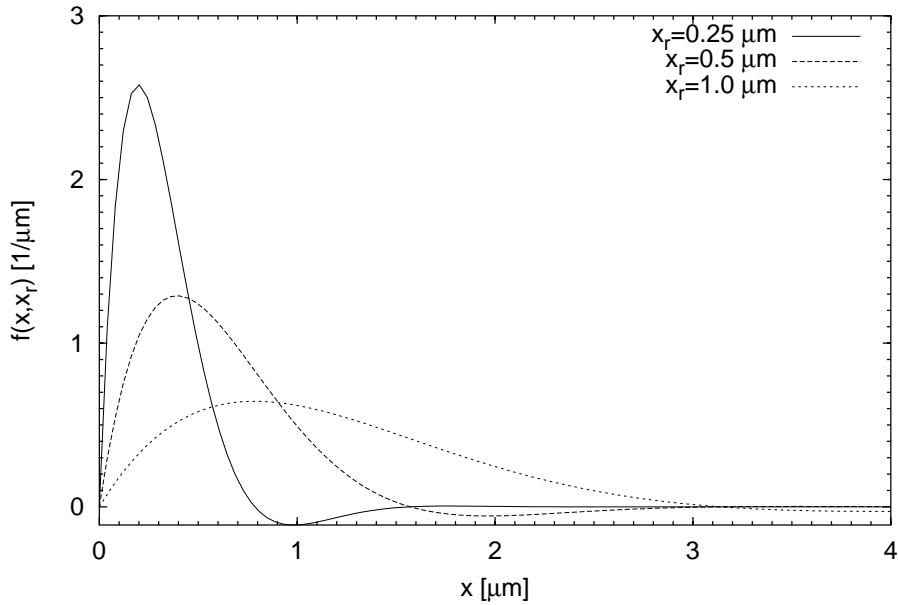
Figure 9: Plot of the scanning function $f(x, x_r)$ for different values of x_r.

the sample, the spatial resolution is insufficient to obtain a meaningful result. Moreover, the approximate solution of the heat conduction equation no longer holds. To obtain a complete depth-profile, we therefore have to do a second measurement from the rear side of the sample.

The spatial resolution can be improved by applying differential operators to Eq. (28). For further details, see Ref. [6].

To summarize, Eqs. (26) and (27) are the basis of our LIMM analysis. For each frequency ω at which a value for the pyroelectric signal has been measured, we simply have to calculate x_r and plot p_a vs. x_r. At this point, we can plot p_a in arbitrary units only. However, in the following section we shall develop a method to calculate absolute values of the pyroelectric coefficient.

3.4 Calibrating the LIMM spectra

If we knew all parameters appearing in Eq. (19), calculation of absolute values of the pyroelectric coefficient would be straightforward. However, we generally do not have an accurate value of the absorption coefficient η (the absorption of the aluminum electrode strongly depends on oxidation, which increases with age). Also, the experiment does not provide an energy detector to measure the modulation amplitude $j_\sim$. With so many unknown quantities, how do we get absolute values for $p(x)$? It turns out that all we need to do is to measure the transient temperature $\Delta T_\sim$ at the heated surface ($x = 0$) [8]. In the experimental section 2.5 we have already see that this measurement is done at low frequencies, where $k_r \ll d^{-1}$ (i.e., the penetration depth x_r is much larger than the

sample thickness). Therefore, we can use the approximate solution of the heat conduction equation (Eq. (10)) which we insert into Eq. (18) to obtain the pyroelectric signal

$$\Re I_\sim = \frac{\eta j_\sim A}{c\rho d} \, p_0 \, , \tag{31}$$

where p_0 is the average pyroelectric coefficient:

$$p_0 = \frac{1}{d} \int_0^d p(x) \, dx \, . \tag{32}$$

Using Eq. (10), we can eliminate $\eta j_\sim$ and obtain

$$p_0 = \frac{\Re I_\sim}{A\omega \, \Im(\Delta T_\sim(x = 0))} \, , \tag{33}$$

where $\Re$ and $\Im$ denote the real and imaginary part, respectively. Here we have taken $\Delta T_\sim$ at the heated surface, since this is where we will eventually measure it.

An important point has to be made here: $I_\sim$ and $T_\sim$ are *amplitudes*, whereas the lock-in amplifier measures *effective values*, which for a sinusoidal oscillation are equal to $1/\sqrt{2}$ times the amplitude. In Eq. (33), we may replace both $\Re I_\sim$ and $\Im(\Delta T_\sim(x = 0))$ with their effective values, since the factors of $\sqrt{2}$ in the numerator and denominator cancel.

As a side note, it should be added that measuring the pyroelectric response as a function of temperature yields important information about the *relaxation* of oriented dipoles. For more information about pyroelectric relaxation spectroscopy, see Refs. [2, 4].

Appendix

A Laser Safety

The experiment makes use of a diode laser emitting red light at a wavelength of 785 nm and a power of 50 mW. According to DIN VDE 0837 it is a category 3b laser. Looking into the beam or specular reflections of it may cause **instant and irreversible eye damage**. Please note that the sensitivity of the human decreases for wavelengths > 700 nm, thus creating the false impression of a "faint" light source.

The experimental setup has been designed such that no direct or specularly reflected laser radiation can escape from the chamber, eliminating the need to wear protective glasses. However, the laser diode **must not be removed** from its mount under any circumstances! Turn off the laser before removing the front cover of the chamber. A microswitch interlock prevents the laser from operating while the cover is not in place.

B Important parameters

Material properties of PVDF

- Heat capacity per volume: $c\rho = 2.3 \times 10^6$ J m^{-3} K^{-1}

- Thermal conductivity: $\kappa = 0.14$ W m^{-1} K^{-1}

Other parameters

- current-to-voltage converter gain: 20 MV/A

- sample diameter: 5 mm

C Computer Commands

C.1 Octave

C.1.1 Overview

Octave is a high-level language for numerical calculations distributed under the GNU Public License. It is largely compatible with the commercial Matlab^{TM} package. For the LIMM experiment, we have written a few programs that will help you simulate temperature distributions, pyroelectric signals and reconstruction of the pyroelectric coefficient from a given signal. Data acquisition, too, can be performed by **Octave**. The available programs are listed in Table 1. The source code of each program has the ending `.m` and can be edited with any text editor (e. g. `joe` or `vi`). Lines starting with `#` are comments. A program can be run by simply typing its file name in the octave window. Some programs will prompt you for additional input.

`temperature`	simulation of temperature distribution using Eqs. (6) and (9)
`pyro`	simulation of the pyroelectric current using Eq. (19)
`reconstruct`	reconstruction of the $p(x)$ distribution using the approximation and regularization methods. The reconstructed pyroelectric distribution and the pyrocurrent can be written to ASCII files (you will be prompted for the file names), which you can take home for plotting.
`analyze`	reconstruction of the $p(x)$ distribution from measured data using the approximation and regularization methods. The data must be supplied as a file containing the frequency (in Hz) and the real and imaginary part of the pyroelectric current in three columns, separated by blanks or tabs. The reconstructed distribution is written to an ASCII file (you will be prompted for the file name).
`gv`	opens up a `ghostview` window with the last plot; from `ghostview`, the plot can be sent to a printer
`limmdac`	data acquisition program. This program scans the modulation frequency and reads out voltages from the lock-in amplifier. However, it needs to be completed by the students as part of this lab exercise.

Table 1: Important *Octave* routines.

C.1.2   Programming with *Octave*

Acquisition of the pyrolectric current data is performed by the `limmdac.m` routine. A listing is shown in Tab. 3. To successfully run the program, you need to add a loop that assigns frequency values to the `frq` variable. Here are a few hints that will help you getting started:

- Use frequencies that are evenly spaced on a logarithmic scale. Record at least 10 data points per factor 10 interval.

- Some important *Octave* commands are listed in Appendix C.1.3. Also, you can get online help by typing `help -i <command>` in the octave command window. (Replace `<command>` by the command you need help for.)

- All octave commands should be terminated with a semicolon (;), or else the result (numerical or string) of the command will be printed on the screen.

C.1.3   Octave commands

`while, endwhile`   execute a loop.
                             Example: `while (x<10)`
                                                `x++;`
                                             `endwhile`

```
for i=<startvalue>:<endvalue>    another way to build a loop.
                        Example:     for i=20:40
                                        x=x+i
                                     endfor
 if, else, endif          conditional statement
                        Example:     if (x>0)
                                        y=x;
                                     else
                                        y=-x;
                                     endif
```

C.2 Editor

We recommend you use the `joe` editor (if you feel more comfortable with `vi` or `emacs`, you are welcome to use them). From the command line, it is invoked via `joe <filename>`. Table 2 lists the most important editor commands.

`Ctrl-k e`	load file
`Ctrl-k s`	save file (confirm with `<Return>`)
`Ctrl-k x`	save file and exit
`Ctrl-c`	quit without saving
`<Backspace>`	delete character left of cursor
`<Del>`	same as `<Backspace>`
`Ctrl-d`	delete character under cursor
`Ctrl-y`	delete line
`Ctrl-k f`	search / replace
`Ctrl-h`	toggle help screen

Table 2: Important keystrokes for the `joe` editor.

D Lock-in Amplifier

The electrical signals encountered in the present experiment are all rather small. For example, typical pyroelectric currents are of the order of 1 nA, and the bolometer output may be as low as 10 nV. If we displayed this signal on an oscilloscope, the pyroelectric current would be completely hidden within a much larger noise. To suppress this noise, we make use of the fact that the pyroelectric signal is modulated at the same frequency as the diode laser (although its phase may be shifted with respect to the laser). A *phase-sensitive* or *lock-in* amplifier isolates these components from the background noise. Fig. 10 shows the basic components of this device.

From Fourier analysis we know that any time-dependent signal can be expanded as a series of periodic functions, $\cos\omega t$ and $\sin\omega t$, where ω assumes arbitrary values between 0 and ∞. Let us find out what happens to a Fourier component proportional to $\cos\omega t$ when

```
# Data acquisition program for the LIMM experiment
#
# Written by Alexander Kremmer and Axel Mellinger, University of Potsdam
# Last change 2000-06-06 by Axel Mellinger
#
1;

# Turn off output pagination
more off

# Clear all variables
clear;

# set serial interface
system("./setcom2");

# Open serial interface. Use /dev/ttyS0 for COM1, /dev/ttyS1 for COM2
fid=fopen("/dev/ttyS1","r+");

# Open output file
k=input("Enter output filename: ", "s");
outfile=fopen(k, "w");
fprintf (outfile,"# %12s %12s %12s\n", "frequency", "U (real)", "U (imag)");

# Set sensitivity to 50 mV
fputs(fid,"sen 17\r");

l=0;  # auxiliary counter

#########################################################################
# Here we need a loop that scans the frequency between 10 Hz and 100 kHz
# with at least 10 data points per order of magnitude. The data points
# should be evenly spaced on a logarithmic frequency scale.

  # begin loop

  frq =      # <------------ Set frequency here

  # Set oscillator frequency
  SetFrequency(fid, frq);

  # Set time constant and wait 3 seconds
  TimeConst(fid,frq);
  sleep(3);

  # Read data from lock-in amplifier
  [VRe, VIm]=GetXY(fid);
  fprintf(outfile, "  %12.5e %12.5e %12.5e\n", frq, VRe, VIm);

  # Compile data into a vector
  l++;
  graph (l,1)=frq; graph (l,2)=VRe; graph (l,3)=VIm;

  # Plot data
  gset xrange[1:1e5];
  gset logscale x
  gplot graph using 1:2 title "U (real)", graph using 1:3 title "U (imag)"

  # end loop
#########################################################################

# Close serial port and output file
fclose(fid);
fclose(outfile);
```

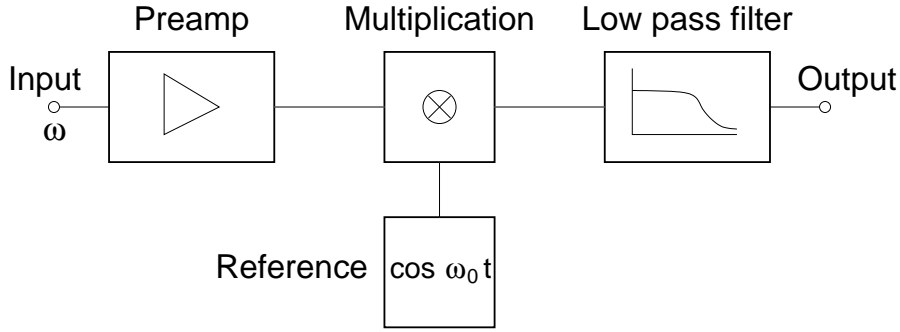Table 3: Program listing of the `limmdac` routine.

Figure 10: Schematic view of a lock-in amplifier. Commercial devices have two separate channels, one multiplying the signal with $\cos \omega_0 t$, the other multiplying it with $\sin \omega_0 t$. This way, the phase of the input signal can be obtained.

we feed it into the lock-in amplifier. After a preamplifier stage, the signal multiplied by a reference signal proportional to $\cos \omega_0 t$. Here, ω_0 is modulation frequency of our diode laser. The product signal is then sent through a low pass filter, which effectively averages the signal over a time t_{LP}, which is significantly larger than $1/\omega_0$. Mathematically, the lock-in amplifier calculates the integral

$$S = \frac{1}{t_{\text{LP}}} \int_0^{t_{\text{LP}}} \cos \omega t \, \cos \omega_0 t \, dt \tag{34}$$

From the theory of complex numbers, we remember that $\cos \omega t$ can be written as

$$\cos \omega t = \frac{e^{i\omega t} + e^{-i\omega t}}{2} \, , \tag{35}$$

which we use to rewrite Eq. (34) as

$$S = \frac{1}{t_{\text{LP}}} \int_0^{t_{\text{LP}}} \left\{ \cos[(\omega + \omega_0)t] + \cos[(\omega - \omega_0)t] \right\} \, dt \, . \tag{36}$$

Both terms under the integral are oscillating functions and therefore vanish when averaged over large times t_{LP}. There is one exception, however: If the frequency of the input signal ω exactly matches ω_0, the second term becomes constant, leading to a non-zero value of the integral. In other words, the lock-in amplfier can isolate *a single frequency component* from an otherwise very noisy signal. In addition, by using a second reference proportional to $\sin \omega_0 t$, it is possible to obtain the *phase* of the input signal relative to the reference channel.

For the LIMM experiment, we use a commercial (EG&G 5110) lock-in amplifier. This device has an internal oscillator, which supplies both the reference signal and the modulation voltage for the laser diode. Its manual is available at the experiment.

E   Calculating the Temperature Phase Lag

The measurement of the transient temperature at the front and back electrode was described on page 10. We define the complex temperature amplitudes as

$$
\begin{aligned}
\Delta T_\sim(x = 0) &= u_\mathrm{r} + iu_\mathrm{i} &= r_1 \exp(i\phi_1) &\qquad \text{(front)} \\
\Delta T_\sim(x = d) &= v_\mathrm{r} + iv_\mathrm{i} &= r_2 \exp(i\phi_2) &\qquad \text{(rear)}
\end{aligned}
$$

According to Eq. (13) the two temperatures differ not only in amplitude, but also in phase. Since

$$
\frac{r_1 \exp(i\phi_1)}{r_2 \exp(i\phi_2)} = \frac{r_1}{r_2} \exp[i(\phi_1 - \phi_2)]
$$

we can obtain the phase difference by calculating

$$
\frac{\Delta T_\sim(x = 0)}{\Delta T_\sim(x = d)} = \frac{u_\mathrm{r} + iu_\mathrm{i}}{v_\mathrm{r} + iv_\mathrm{i}} = \frac{u_\mathrm{r}v_\mathrm{r} + u_\mathrm{i}v_\mathrm{i} - i(u_\mathrm{i}v_\mathrm{r} - u_\mathrm{r}v_\mathrm{i})}{v_\mathrm{r}^2 + v_\mathrm{i}^2} \tag{37}
$$

and

$$
\tan(\Delta\phi) = \frac{u_\mathrm{i}v_\mathrm{r} - u_\mathrm{r}v_\mathrm{i}}{u_\mathrm{r}v_\mathrm{r} + u_\mathrm{i}v_\mathrm{i}} . \tag{38}
$$

With increasing laser modulation frequency, the phase angle will grow from 0 to arbitrarily large values. However, solving Eq. (38) for $\Delta\phi = \arctan(\ldots)$ will produce a *discontinuous* result, since the arctan function jumps by $-\pi$ each time the phase angle passes through $\pi/2$, $3\pi/2$, $5\pi/2$, etc. Therefore, multiples of π must be added to obtain a continuous function $\Delta\phi(\omega)$.

F   Linear Regularization Methods (Optional)

In this section we look at an approach for solving the ill-conditioned Fredholm integral of Eq. (19) which does not rely on an approximate solution of the heat conduction equation. As briefly mentioned in Section 3.2, the strategy of *regularization* techniques is to impose additional constraints in order to make the solution unique. A more detailed discussion of these techniques can be found in Ref. [9].

We start with the (complex) values of the pyroelectric current I_ν, $\nu = 1 \ldots N$, measured at the frequencies ω_ν. The goal is to calculate the pyroelectric coefficient $p(x)$ at the $M+1$ points x_μ, $\mu = 0 \ldots M$. Typically, M is of the order of 200 or more. Since we want to calculate $p(x)$ at discrete points, we must find a way to bring the integral in Eq. (19) into a discrete form. This is done using the trapezoid rule for numerical integration.

We approximate the integral

$$
F = \int_{x_0}^{x_M} f(x)\, dx
$$

by the sum of the areas of the trapezoids between x_μ and $x_{\mu+1}$, as shown in Fig. 11. Therefore, we can write

$$
I \approx \frac{f(x_0) + f(x_1)}{2}(x_1 - x_0) + \frac{f(x_1) + f(x_2)}{2}(x_2 - x_1) + \ldots
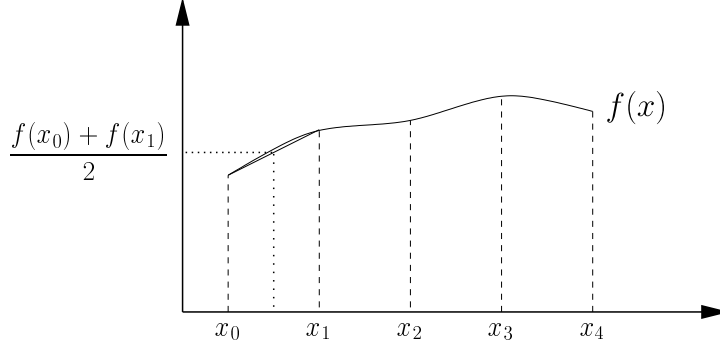$$

Figure 11: Numerical intergration using the trapezoid rule with $M = 4$.

$$+ \frac{f(x_{M-1}) + f(x_M)}{2}(x_M - x_{M-1}) \tag{39}$$

$$= f(x_0)\frac{x_1 - x_0}{2} + f(x_1)\frac{x_2 - x_0}{2} + f(x_2)\frac{x_3 - x_1}{2} + \ldots$$

$$+ f(x_{M-1})\frac{x_M - x_{M-2}}{2} + f(x_M)\frac{x_M - x_{M-1}}{2} \tag{40}$$

Applying this rule to Eq. (19), we can rewrite the integral as a set of linear equations:

$$I_\nu = \sum_{\mu=0}^{M} R_{\nu\mu}p_\mu \,, \tag{41}$$

where

$$R_{\nu\mu} = \frac{A}{d}\frac{\eta j_\sim}{c\rho}\frac{k_\nu}{\sinh(k_\nu d)} \cosh[k_\nu(d - x_\mu)] \times \begin{cases} (x_{\mu+1} - x_\mu)/2 & ; \mu = 0 \\ (x_{\mu+1} - x_{\mu-1})/2 & ; 1 \le \mu \le M - 1 \\ (x_\mu - x_{\mu-1})/2 & ; \mu = M \end{cases} \tag{42}$$

and (cf. Eqs. (7–8))

$$k_\nu = (1 + i)\sqrt{\omega_\nu/2D} \,. \tag{43}$$

This somewhat complicated equation takes into account the borders at $\mu = 0$ and M. Note that I_ν and $R_{\nu\mu}$ are complex quantities, but the p_μ are real numbers.

We have yet to decide on a suitable set of x_m. The straightforward choice is a set of equidistant points. However, the oscillatory behavior of the hyperbolic sine and cosine functions in Eq. (19) at high frequencies requires a large number of intervals near $x = 0$ in order to minimize the numerical error. Therefore, we choose as x_m a set of points evenly spaced on a logarithmic scale, i. e.

$$x_m = \begin{cases} 0 & ; \mu = 0 \\ x_M/z^{M-m} & ; 1 \le \mu \le M \end{cases} . \tag{44}$$

Typically, z is chosen so that we have about 40 points per decade.

To solve for the unknown p_μ, one could try to minimize the differences between the observed and calculated I_ν:

$$\chi^2[\mathbf{p}] = \sum_\nu \left| \frac{I_\nu - \sum_{\mu=0}^{M} R_{\nu\mu} p_\mu}{\sigma_\nu} \right|^2 \stackrel{!}{=} \min . \tag{45}$$

In matrix notation, we can write this expression in the more compact form of

$$(\mathbf{b} - \mathbf{Ap})^\dagger (\mathbf{b} - \mathbf{Ap}) = \min \tag{46}$$

(the operator † denotes the transpose, complex conjugate matrix, i. e. $\mathbf{A}^\dagger = \tilde{\mathbf{A}}^*$). The $N \times M$ matrix $\mathbf{A}$ and the column vector $\mathbf{b}$ are defined as $A_{\nu\mu} = R_{\nu\mu}/\sigma_\nu$ and $b_\nu = I_\nu/\sigma_\nu$, respectively. This approach does not really work, since in general $\mathbf{A}$ has more columns (M) than rows (N), so that we are left with more unknowns than equations. However, we can get a unique solution if we impose another condition $\mathcal{B}$, which we seek to minimize together with χ^2:

$$\chi^2[\mathbf{p}] + \lambda \mathcal{B}[\mathbf{p}] = \min . \tag{47}$$

The parameter λ is a weight factor that determines whether the minimization of χ^2 or $\mathcal{B}$ has the greater priority.

As an example, let us assume that we are looking for a solution which is nearly a constant. Hence, we define $\mathcal{B}$ as the sum of squares of the differences between adjacent p_μ:

$$\mathcal{B}[\mathbf{p}] = |\mathbf{B} \cdot \mathbf{p}|^2 = \tilde{\mathbf{p}}(\mathbf{B}^\dagger \mathbf{B})\mathbf{p} = \tilde{\mathbf{p}}\mathbf{Hp} \tag{48}$$

with

$$\mathbf{B} = \begin{pmatrix} -1 & 1 & 0 & 0 & 0 & 0 & 0 & \cdots & 0 \\ 0 & -1 & 1 & 0 & 0 & 0 & 0 & \cdots & 0 \\ 0 & 0 & -1 & 1 & 0 & 0 & 0 & \cdots & 0 \\ \vdots & & & & \ddots & & & & \vdots \\ 0 & \cdots & 0 & 0 & 0 & -1 & 1 & 0 & 0 \\ 0 & \cdots & 0 & 0 & 0 & 0 & -1 & 1 & 0 \\ 0 & \cdots & 0 & 0 & 0 & 0 & 0 & -1 & 1 \end{pmatrix} \tag{49}$$

and

$$\mathbf{H} = \begin{pmatrix} 1 & -1 & 0 & 0 & 0 & 0 & 0 & \cdots & 0 \\ -1 & 2 & -1 & 0 & 0 & 0 & 0 & \cdots & 0 \\ 0 & -1 & 2 & -1 & 0 & 0 & 0 & \cdots & 0 \\ \vdots & & & & \ddots & & & & \vdots \\ 0 & \cdots & 0 & 0 & 0 & -1 & 2 & -1 & 0 \\ 0 & \cdots & 0 & 0 & 0 & 0 & -1 & 2 & -1 \\ 0 & \cdots & 0 & 0 & 0 & 0 & 0 & -1 & 1 \end{pmatrix} \tag{50}$$

The expression to be minimized is

$$(\mathbf{b} - \mathbf{Ap})^\dagger (\mathbf{b} - \mathbf{Ap}) + \lambda \tilde{\mathbf{p}}\mathbf{Hp} = \min \tag{51}$$

We know that we are at a local extremal point when the partial derivatives with respect to the components p_μ of $\mathbf{p}$ vanish. With some algebraic rearrangements and the definition

$$\mathbf{X} = \mathbf{A}^\dagger \mathbf{A} + \lambda \mathbf{H} \tag{52}$$

we thus obtain the linear set of equations

$$(\tilde{\mathbf{X}} + \mathbf{X})\mathbf{p} = \mathbf{A}^\dagger \mathbf{b} + \tilde{\mathbf{A}} \mathbf{b}^* \,. \tag{53}$$

Solving Eq. (53) yields the functional form of p.

We have yet to decide the optimum value for λ. Obviously, setting $\lambda = 0$ brings us back to the undetermined set of equations (46), while a large λ gives us a constant solution – exactly as has been required by the choice of $\mathbf{B}$ in Eq. (49). A good "first guess" is the value that makes both terms in Eq. (52) of equal magnitude:

$$\lambda = \mathrm{Tr}(\mathbf{A}^\dagger \mathbf{A})/\mathrm{Tr}(\mathbf{H}) \tag{54}$$

When λ is chosen too small, the solution will be unstable and shows strong oscillations. If λ is too large, the solution will be over-simplified by the constraint $\mathcal{B}$. Statistical theory gives gives us more formal criteria to determine the optimum value of λ; however, these techniques are beyond the scope of this tutorial. For our purposes, it is sufficient to optimize λ "by hand", i. e. try different values until the reconstructed pyroelectric distribution looks "convincing".

Problem 4 *The depth-profile of the pyroelectric coefficient is generally not a constant function, so that Eq. (49) is an unsuitable constraint. Rather, we are looking for "smooth" solutions with a low curvature. Which constraint $\mathcal{B}[\mathbf{p}]$ could produce such a solution? Set up the matrices $\mathbf{B}$ and $\mathbf{H}$!*

References

[1] S. Bauer, "Poled polymers for sensors and applicatios," *J. Appl. Phys.* **80**, pp. 5531–5558, 1996.

[2] S. Bauer and S. B. Lang, "Pyroelectric polymer electrets," *IEEE Trans. Dielectr. Electr. Insul.* **3**, pp. 647–676, 1996.

[3] S. Bauer, S. Bauer-Gognea, S. Yilmaz, W. Wirges, and R. Gerhard-Multhaupt, "Pyro-electrical investigation of nonlinear optical polymers with uniform or patterned dipole orientation," in *Polymers for Second-Order Nonlinear Optics*, G. A. Lindsay and K. D. Singer, eds., vol. 75, pp. 304–316, ACS Symposium Series, 1994.

[4] S. Bauer, "Pyroelectrical investigation of charged and poled nonlinear optical polymers," *J. Appl. Phys.* **75**, pp. 5306–5315, 1994.

[5] "Meßwiderstand Pt 100 nach DIN IEC 751." (table available in room 1.21).

[6] B. Ploss, R. Emmerich, and S. Bauer, "Thermal wave probing of pyroelectric distributions in the surface region of ferroelectric materials: A new method for the analysis," *J. Appl. Phys.* **72**, pp. 5363–5370, 1992.

[7] S. B. Lang, "Laser intensity modulation method (LIMM): Experimental techniques, theory and solution of the integral equation," *Ferroelectrics* **118**, pp. 343–361, 1991.

[8] S. Bauer and B. Ploss, "A method for the measurement of the thermal, dielectric, and pyroelectric properties of thin pyroelectric films and their applications," *J. Appl. Phys.* **68**, pp. 6361–6367, 1990.

[9] W. H. Press, B. P. Flannery, S. A. Teukolsky, and W. T. Vetterling, *Numerical Recipes in FORTRAN 77*, Cambridge University Press, Cambridge, 2nd ed., 1992. Free online access at `http://www.nr.com`.

Note: The referenced papers can be borrowed for copying from the instructor.